Synthesis, structure and imaging of oligodeoxyribonucleotides with tellurium-nucleobase derivatization

Jia Sheng[1], Abdalla E. A. Hassan[1,2], Wen Zhang[1], Jianfeng Zhou[3], Bingqian Xu[3], Alexei S. Soares[4] and Zhen Huang[1,*]

[1]Department of Chemistry, Georgia State University, Atlanta, GA 30303, USA, [2]Applied Nucleic Acids Research Center, Zagazig University, Zagazig, Egypt, [3]Faculty of Engineering and NanoSEC, University of Georgia, Athens, GA 30602 and [4]Department of Biology, Brookhaven National Laboratory, Upton, NY 11973, USA

ABSTRACT

We report here the first synthesis of 5-phenyl–telluride–thymidine derivatives and the Te-phosphoramidite. We also report here the synthesis, structure and STM current-imaging studies of DNA oligonucleotides containing the nucleobases (thymine) derivatized with 5-phenyl-telluride functionality (5-Te). Our results show that the 5-Te-DNA is stable, and that the Te-DNA duplex has the thermo-stability similar to the corresponding native duplex. The crystal structure indicates that the 5-Te-DNA duplex structure is virtually identical to the native one, and that the Te-modified T and native A interact similarly to the native T and A pair. Furthermore, while the corresponding native showed weak signals, the DNA duplex modified with electron-rich tellurium functionality showed strong topographic and current peaks by STM imaging, suggesting a potential strategy to directly image DNA without structural perturbation.

INTRODUCTION

Well-behaved base pair recognitions and duplex structures of DNAs and RNAs have stimulated extensive research investigations, such as DNA nano-structure construction and self-assembling (1–4), disease and pathogen detection at single molecule level (5), oligonucleotide drug discovery (6) and nanoelectronic device design based on DNA conductivity and charge migration (7–12). Moreover, chemical modifications of nucleobases have been widely used to selectively tailor the chemical and biophysical properties of DNAs and RNAs and to probe their chemical and biochemical functions, including base pairing specificity, polymerase recognition, DNA damaging and repairing (13–19) and DNA current/conductivity imaging, including metallization and conjugating with conductive nanoparticles or polymers through scanning tunneling microscopy (STM) to image DNA (20–24).

Tellurium, which was recently introduced to the sugar moiety of the nucleosides and nucleotides (25,26), is a non-metal element with a much larger atomic size (atomic radius: 1.40 Å) (27) in the same elemental family of oxygen (0.73 Å), sulfur (1.02 Å) and selenium (1.16 Å) (28). Tellurium has much higher metallic property and stronger electron delocalizability than the other ones in the same elemental family. Since DNA duplexes are relatively electron deficient, we hypothesize that an electron-rich tellurium atom will likely donate electron and facilitate electron delocalization and DNA imaging, when it is introduced into DNA duplexes via the nucleobases.

Herein, we report the first synthesis of a tellurium-nucleobase-derivatized nucleoside (Te-thymidine or [Te]T), the Te-phosphoramidite and Te-DNAs. We found that the [Te]T-DNA duplex has the thermo-stability similar to the corresponding native duplex. Furthermore, our X-ray crystal structure studies of the Te-derivatized DNAs indicate that the Te-derivatized and native structures are virtually identical, and that [Te]T and A interact as well as the native T–A pair. Moreover, our STM imaging study reveals that the Te-DNAs show strong characteristic current peaks on graphite surface, suggesting a useful DNA imaging strategy without perturbation of the local and global structures.

MATERIALS AND METHODS

Synthesis of 5-TePh-thymidine phosphoramidite

3′-O-tert-butyldimethylsilyl-5′-O-(4,4-dimethoxytrityl)-2′-deoxy-5-iodouridine (2). Tert-butyldimethylsilyl chloride

*To whom correspondence should be addressed. Tel: +1 404 413 5535; Fax: +1 404 413 5535; Email: Huang@gsu.edu

(TBDMSCl) (0.344 g, 2.3 mmol) was added to a mixture of $5'$-O-(4,4-dimethoxytrityl)-$2'$-deoxy-5-iodouridine (**1**, 1 g, 1.52 mmol) and imidazole (0.3 g, 4.6 mmol) in anhydrous DMF (10 ml). The mixture was stirred at room temperature for 1.5 h, and then quenched with MeOH. The mixture was diluted with EtOAc (30 ml) and washed with H_2O (3 × 10 ml) and brine. The organic phase was dried over anhydrous $MgSO_4$ (s) and the solvents were evaporated under reduced pressure. The residue was purified by a flash silica gel column (eluent: 20% EtOAc in hexanes) to give **2** (1.15 g, 98%): ^{1}H-NMR (CDCl$_3$, δ): 9.21 (1H, br, NH, exchangeable with D_2O), 8.22 (1H, s, H-6), 7.46–7.35 (9H, m, Ar), 6.89–6.86 (4H, m, Ar), 6.31 (1H, dd, H-$1'$, J = 5.9, 7.5 Hz), 4.49 (1H, m, H-$3'$), 4.15 (1H, m, H-$4'$), 3.82 (6H, 2s, CH$_3$O), 3.45 (1H, dd, H-$5'$a, J = 2.7, 10.8 Hz), 3.32 (1H, dd, H-$5'$b, J = 3.1, 10.8 Hz), 2.42 (1H, ddd, H-$2'$a, J = 2.7, 5.8, 13.3 Hz), 2.20 (1H, m, H-$2'$b), 0.87 (9 H, 3 s, SiMe$_3$), 0.05–0.002 (6H, 2s, SiMe$_2$); ^{13}C-NMR (CDCl$_3$) δ 160.41 (C4), 158.67 (Ar), 150.23 (C2), 144.37 (C-6), 144.33 (Ar), 135.54 (Ar), 135.46 (Ar), 130.13 (Ar), 130.08 (Ar), 128.10 (Ar), 127.06 (Ar), 113.39 (Ar), 87.29 (C$4'$), 86.96 (Ar), 85.85 (C-$1'$), 72.43 (C-$3'$), 68.66 (C-5), 63.03 (H$5'$), 55.27 (OMe), 42.00 (C$2'$), 25.78 (C$\underline{C}$H$_3$), 17.97 ($\underline{C}$CH$_3$), −4.63 (Si$\underline{C}$H$_3$), −4.84 (Si$\underline{C}$H$_3$); HRMS (ESI-TOF): molecular formula: C$_{36}$H$_{42}$N$_2$O$_7$Si; [M-H]$^+$: 769.1800 (Figure S5; calcd 769.1806)

$3',5'$-Di-O-tert-butyldimethylsilyl-$2'$-deoxy-5-iodouridine (**4**).

TBDMSCl (1.28 g, 8.43 mmol) was added to a mixture of 5-iodo-$2'$-deoxyuridine (**3**, 1 g, 2.81 mmol) and imidazole (1.3 g, 8.5 mmol) in anhydrous DMF (10 ml). The mixture was stirred at room temperature for 2 h, and then quenched with MeOH. The mixture was diluted with EtOAc (30 ml) and washed with H_2O (3 × 10 ml) and brine. The organic phase was dried over anhydrous $MgSO_4$ (s) and the solvents were evaporated under reduced pressure. The residue was purified by a flash silica gel column (eluent: 30% EtOAc in hexanes) to give **4** (1.34 g, 99%) as white foam: ^{1}H-NMR (CDCl$_3$, δ): 9.35 (1H, br, NH, exchangeable with D_2O), 8.06 (1H, s, H-6), 6.26 (1H, dd, H-$1'$, J = 5.7, 7.9 Hz), 4.38 (1H, m, H-$3'$), 3.97 (1H, m, H-$4'$), 3.86 (1H, dd, H-$5'$a, J = 2.2, 11.5 Hz), 3.76 (1H, dd, H-$5'$b, J = 2.4, 11.5 Hz), 2.30 (1H, ddd, H-$2'$a, J = 2.3, 5.7, 13.1 Hz), 1.98 (1H, m, H-$2'$b), 0.93 (9 H, s, SiCMe$_3$), 0.88 (9 H, s, SiCMe$_3$), 0.14–0.06 (12 H, 4s, SiMe$_2$); ^{13}C-NMR (DMDO-d$_6$) δ 160.50 (C4), 150.34 (C2), 144.51 (C-6), 88.49 (C$4'$), 88.13 (C-$1'$), 72.60 (C-$3'$), 68.69 (C5), 63.14 (C-$5'$), 41.70 (C$2'$), 26.47 (C$\underline{M}$e$_3$), 25.89 (C$\underline{M}$e$_3$), 18.95 (C$\underline{M}$e$_3$), 18.12 (C$\underline{M}$e$_3$), −4.50 (SiMe$_2$), −4.70 (SiMe$_2$), −4.83 (SiMe$_2$), −4.96 (SiMe$_2$); HRMS (ESI-TOF): molecular formula: C$_{21}$H$_{40}$N$_2$O$_5$ISi$_2$; [M+H]$^+$: 583.1525 (Figure S4; calcd 583.1521).

$3',5'$-Di-O-tert-butyldimethylsilyl-$2'$-deoxy-5-phenyltellurouridine (**5**).

NaH 95% (6 mg, 0.25 mmol) was added to a solution of **4** (0.15 g, 0.25 mmol) in dry THF (1 ml) at room temperature in dry glove box. The mixture was stirred for 30 min until complete cease of hydrogen gas evolution, then cooled down to −78°C. n-BuLi (0.36 ml, 2.3 M solution in hexanes; 0.83 mmol) was added dropwise over

5 min. The mixture was stirred for 30 min, and then treated with (Ph)$_2$Te$_2$ (0.25 g, 0.75 mmol). The mixture was further stirred for 1 h at the same temperature (−78°C). NaCl (5 ml, saturated aqueous solution) was added, the reaction flask was placed at room temperature and allowed to warm up naturally to the room temperature. Water (10 ml) was added to the flask and EtOAc (3 × 20 ml) was used to extract the crude product. The organic phase was dried over $MgSO_4$, and evaporated under reduce pressure. The residue was purified by flash silica gel chromatography (eluent: 40% EtOAc in hexane containing 1% Et$_3$N) to give **5** (106 mg, 64%) as a colorless foam. Elution with 50% EtOAc in hexane gave **9** (33 mg, 29%) as a colorless foam. Spectral data for **7**: ^{1}H-NMR (CDCl$_3$, δ): 8.64 (1H, br, NH, exchangeable with D_2O), 7.82 (1H, s, H-6), 7.81–7.78 (2H, m, Ar), 7.33–7.24 (3H, m, Ar), 6.25 (1H, dd, H-$1'$, J = 5.6, 8.0 Hz), 4.31 (1H, m, H-$3'$), 3.92 (1H, m, H-$4'$), 3.63–3.54 (2H, m, H-$5'$a,b), 2.30 (1H, ddd, H-$2'$a, J = 2.4, 5.6, 13.2 Hz), 1.94 (1H, m, H-$2'$b), 0.90 (9 H, s, SiCMe$_3$), 0.88 (9 H, s, SiCMe$_3$), 0.09–0.07 (12 H, 4s, SiMe$_2$); ^{13}C-NMR (DMDO-d$_6$) δ 162.65 (C4), 150.21 (C2), 149.77 (C-6), 138.62 (Ar), 129.56 (Ar), 128.41 (Ar), 113.08 (C-5), 89.12 (Ar), 88.48 (C$4'$), 85.85 (C-$1'$), 72.57 (C-$3'$), 63.16 (C-$5'$), 42.04 (C$2'$), 26.18 (C$\underline{M}$e$_3$), 26.08 (C$\underline{M}$e$_3$), 18.42 (C$\underline{M}$e$_3$), 18.42 (C$\underline{M}$e$_3$), −4.48 (SiMe$_2$), −4.66 (SiMe$_2$); HRMS (ESI-TOF): molecular formula: C$_{27}$H$_{43}$N$_2$O$_5$Si$_2$Te; [M-H$^+$]$^-$: 661.1775 (Figure S6; calcd 661.1773).

$3'$-O-tert-Butyldimethylsilyl-$5'$-O-(4,4-dimethoxytrityl)-$2'$-deoxy-5-phenyltellurouridine (**6**).

NaH 95% (19 mg, 0.67 mmol) was added portion wise to a solution of **2** (0.516 g, 0.67 mmol) in dry THF (2 ml) at room temperature in dry glove box. The mixture was stirred for 30 min until complete cease of hydrogen gas evolution, then cooled down to −78°C and treated with n-BuLi (1.0 ml, 2.3 M solution in hexane; 2.3 mmol) dropwise over 10 min. The mixture was stirred for 30 min, and then treated with (Ph)$_2$Te$_2$ (0.75 g, 1.8 mmol). The mixture was further stirred for 1 h at the same temperature (−78°C). NaCl (10 ml, saturated aqueous solution) was added, the reaction flask was placed at room temperature and allowed to warm up naturally to the room temperature. Water (10 ml) was added to the flask and EtOAc (3 × 20 ml) was used to extract the crude product. The organic phase was dried over $MgSO_4$ (s), and evaporated under reduce pressure. The residue was purified by flash silica gel chromatography (eluent: 40% EtOAc in hexanes containing 1% Et$_3$N) to give **6** (0.39 g, 68%) as a colorless foam. Elution with 50% EtOAc in hexanes gave **8** (108 mg, 25%) as a colorless foam. Spectral data for **6**: ^{1}H-NMR (CDCl$_3$, δ): 9.42 (1H, br, NH, exchangeable with D_2O), 7.92 (1H, s, H-6), 7.70–6.86 (18H, m, Ar), 6.29 (1H, dd, H-$1'$, J = 6.4, 8.0 Hz), 4.27 (1H, m, H-$3'$), 3.99 (1H, m, H-$4'$), 3.81 (6H, 2 s, CH$_3$O), 3.25 (2H, m, H-$5'$a,b), 2.37 (1H, ddd, H-$2'$a, J = 2.4, 5.6, 13.2 Hz), 2.08 (1H, m, H-$2'$b), 0.87 (9 H, 3 s, SiMe$_3$), 0.09–0.05 (12 H, 4s, SiMe$_2$); HRMS (ESI-TOF): molecular formula: C$_{42}$H$_{48}$N$_2$O$_7$TeSi; [M + H$^+$]$^+$: 851.2357 (Figure S1; calcd 851.2371).

5′-O-(4,4-dimethoxytrityl-2′-deoxy-5-phenyltellurouridine (7). TBAF (0.5 ml, 1 M solution in THF) was added to a solution of **6** (0.26 g, 0.33 mmol) in THF (5 ml) at 0°C. The mixture was stirred for 3 h at room temperature. The solvent was evaporated and the residue was partitioned between EtOAc and H_2O. The organic phase was dried over anhydrous $MgSO_4$ (s) before evaporation. The residue was purified by silica gel column chromatography (the silica gel was pre-equalized with 1% Et_3N in CH_2Cl_2; eluent: 4% MeOH in CH_2Cl_2) to give (0.2 g, 84%) of seven as pale yellow foam (Figure S7). ^1H-NMR ($CDCl_3$, δ): 9.25 (1H, br, NH, exchangeable with D_2O), 7.83 (1H, s, H-6), 7.62–7.01 (15 H, m, Ar), 6.86–6.82 (4H, m, Ar), 6.23 (1H, dd, H-1′, J = 6.4, 6.8 Hz), 4.34 (1H, m, H-3′), 3.98 (1H, m, H-4′), 3.76 (6H, 2 s, CH_3O), 3.29 (1H, dd, H-5′a, J = 4.4, 10.4 Hz), 3.18 (1H, dd, H-5′b, J = 4.4, 10.8 Hz), 2.40 (1H, ddd, H-2′a, J = 3.6, 6.0, 13.6 Hz), 2.16 (1H, m, H-2′b); ^{13}C-NMR (DMSO-d_6) δ 163.40 (C4), 159.33 (Ar), 151.06 (C2), 147.64 (C-6), 145.31 (Ar), 138.41 (Ar), 136.30 (Ar), 136.67 (Ar), 130.64 (Ar), 130.02 (Ar), 128.67 (Ar), 128.60 (Ar), 128.57 (Ar), 127.54 (Ar), 113.95 (C-5), 113.81 (Ar), 89.62 (Ar), 87.33 (Ar), 86.44 (C4′), 85.72 (C-1′), 72.82 (C-3′), 64.26 (C-5′), 55.81 (OMe), 41.35 (C2′); HRMS (ESI-TOF): molecular formula: $C_{36}H_{33}N_2O_7Te$; $[M]^+$: 735.1342 (Figure S2; calcd 735.1350).

1-[2′-deoxy-3′-O-(2-cyanoethyl-N,N-diisopropylamino)-phosphoramidite-5′-O-(4,4-dimethoxytrityl-β-D-erythro-ribofuranosyl]-5-phenyltellurouridine (10). Disopropylethylamine (44 µl, 0.25 mmol) and *N,N*-diisopropylamino cyanoethylphosphamidic chloride (57 mg, 0.24 mmol) were added to a solution of **7** (0.15 g, 0.2 mmol) in CH_2Cl_2 (2 ml) at 0°C. The mixture was stirred for 2 h at room temperature, and then was slowly poured into pentane (100 ml) under vigorous stirring. The produced white precipitate was filtered out, dissolved in CH_2Cl_2 (1 ml) and re-precipitated in pentane. The collected fine white powder was dried under reduced pressure to give 142 mg **10** (75% yield) as a mixture of two diastereomers, which was directly used for solid phase synthesis without further purification. ^{31}P-NMR (Figure S8, $CDCl_3$, δ): 149·3, 149·8: HRMS (ESI-TOF): molecular formula: $C_{45}H_{51}N_4O_8PTe$; $[M-H^+]^-$: 935.257 (Figure S3; calcd 935.242).

Synthesis of the 5-Te-functionalized DNA

All the DNA oligonucleotides were chemically synthesized in a 1.0 µmol scale using an ABI392 or ABI3400 DNA/RNA Synthesizer. The ultra-mild nucleoside phosphoramidite reagents were used in this work (Glen Research). The concentration of the Te-uridine phosphoramidite was identical to that of the conventional ones (0.1 M in acetonitrile). Coupling was carried out using a 5-(benzylmercapto)-1H-tetrazole (5-BMT) solution (0.25 M) in acetonitrile. The coupling time was 25 s for both native and modified samples. Trichloroacetic acid (3%) in methylene chloride was used for the 5′-detritylation. Synthesis were performed on control pore glass (CPG-500) immobilized with the

appropriate nucleoside through a succinate linker. All the oligonucleotides were prepared with DMTr-on form. After synthesis, the DNA oligonucleotides were cleaved from the solid support and fully deprotected by the treatment of 0.05 M K_2CO_3 solution in methanol for 8 h at room temperature. The 5′-DMTr deprotection was performed in a 3% trichloroacetic acid solution for 2 min, followed by neutralization to pH 7.0 with a freshly made aqueous solution of triethylamine (1.1 M) and extraction by petroleum ether to remove DMTr-OH.

HPLC analysis and purification

The Te-DNA oligonucleotides were analyzed and purified by reverse phase high performance liquid chromatography (RP-HPLC) both DMTr-on and DMTr-off. Purification was carried out using a 21.2×250 mm Zorbax, RX-C8 column at a flow rate of 10 ml/min. Buffer A consisted of 20 mM triethylammonium acetate (TEAAc, pH 7.2), while buffer B contained 50% aqueous acetonitrile and 10 mM TEAAc, pH 7.1. Similarly, analysis was performed on a Zorbax SB-C18 column (4.6×250 mm) at a flow of 1.0 ml/min using the same buffer system. The DMTr-on oligonucleotides were eluded with up to 100% buffer B in 20 min in a linear gradient, while the DMTr-off oligonucleotides were eluted with up to 70% of buffer B in a linear gradient in the same period of time. The collected fractions were lyophilized; the purified compounds were re-dissolved in water. The pH was adjusted to 7.0 after the final purification of the Te-oligonucleotides without the DMTr group.

Thermodenaturization of duplex DNAs

Solutions of the duplex DNAs (2 µM) were prepared by dissolving the DNAs in a buffer containing NaCl (50 mM), sodium phosphate (10 mM, pH 7.2), EDTA (0.1 mM) and $MgCl_2$ (2 mM). The solutions were then heated to 90°C for 3 min, cooled slowly to room temperature and stored at 4°C overnight before measurement. Prior to thermal denaturation, argon was bubbled through the samples. Each denaturing curves were acquired at 260 nm by heating and cooling for four times in a rate of 0.5°C/min using Cary-300 UV–visible spectrometer equipped with temperature controller system.

Crystallization

The purified oligonucleotides (1 mM) were heated to 70°C for 2 min, and cooled slowly to room temperature. The 2′-Se–dU was incorporated into the Te-DNA for the crystallization facilitation. Both native buffer and Nucleic Acid Mini Screen Kit (Hampton Research) were applied to screen the crystallization conditions with l mM of DNA sample at different temperatures using the hanging drop method by vapor diffusion.

Data collection

Glycerol (30%), PEG 400 or the perfluoropolyether was used as a cryoprotectant during the crystal mounting, and data collection was taken under nitrogen gas at 99°K. The Te-DNA-8-mer crystal data were collected at beam line

X12C in NSLS of Brookhaven National Laboratory. A number of crystals were scanned to find the one with strong anomalous scattering at the K-edge absorption of selenium. The distance of the detector to the crystals was set to 150 mm. The wavelengths of 0.9795 Å was chosen for data collection. The crystals were exposed for 10–15 s per image with 1° oscillation, and a total of 180 images were taken for each data set. All the data were processed using HKL2000 and DENZO/SCALEPACK (29).

Structure determination and refinement

The crystal structure of Te-DNA-8-mer was solved by molecular replacement with Phaser (30) using the automated search mode, followed by the refinement of selenium and tellurium atom positions in both CNS (31) and Refmac 5.0 (32). The refinement protocol includes simulated annealing, positional refinement, restrained B-factor refinement and bulk solvent correction. The stereo-chemical topology and geometrical restrain parameters of DNA/RNA (33) have been applied. The topologies and parameters for modified dU with $2'$-SeMe (UMS) and 5-tellurium (TTE) were constructed and applied. After several cycles of refinement, a number of highly ordered waters were added. Final, the occupancies of selenium and tellurium were adjusted. Cross-validation (34) with a 5–10% test set was monitored during the refinement. The σA-weighted maps (35) of the $(2m|F_o| - D|F_c|)$ and the difference $(m|F_o| - D|F_c|)$ density maps were computed and used throughout the model building.

Mass analysis of Te–C bond breaking caused by X-ray irradiation

In our work, a few crystals were analyzed by MALDI-TOF MS before X-ray irradiation. As a comparison, a few crystals were analyzed by MALDI-TOF MS after X-ray irradiation. This Te-functionality is relatively stable in the absence of X-ray irradiation, and no significant decomposition was observed in 2 months under air. The Te-DNA was also heated at 90°C over 1 h without significant decomposition.

STM experiment

In this work, highly oriented pyrolytic graphite (HOPG) was used as a support substrate to study DNA molecules (36). The HOPG was freshly cleaved with scotch tapes prior to each experiment, and treated with UV Surface Decontamination System (Novascan Technologies Inc.) for 20 min before modifying the surface of the hydrophobic HOPG to the hydrophilic surface. The bare HOPG surface did not show obvious structure changes even at the atomic level. Both the native and ^{Te}T-DNA samples (100 μl, 0.03 μM) were dissolved in PBS solution, and the sample solutions were then loaded on the HOPG surface. After 20 min, the DNA samples were scanned with STM in the PBS buffer. To reduce the influence of the leakage current, the newly cut Au STM tip was coated with Apiezon W Wax (SPI Supplies Division of Structure

Probe Inc.), and only the top of the tip was exposed as reported by Lindsay (37).

RESULTS AND DISCUSSION

Synthesis of 5-TePh-thymidine phosphoramidite

Aryl-chalcogenides (S and Se), such as phenyl sulfenyl and phenyl selenyl moieties, have been tethered to the 5-position of pyrimidine nucleosides and been incorporated into DNA (38–41). Methods, which are available in the literature for the introduction of the alkyl or aryl chalcogenides (S and Se) at the 5-position of pyrimidines, include the electrophillic addition–elimination on the C5–C6 double bond (42), the palladium-catalyzed nucleophillic substitution of 5-mercururio derivatives (39,43), and the lithiation of 5-halo derivatives in the presence of the electrophilic species (44). However, no literature report can be found on the corresponding 5-aryl- or alkyl-tellurides. Incorporation of the tellurium functionality to the 5-position is a long-standing challenge. We have attempted, without success, to introduce an alkyltelluro or aryltelluro moiety at the 5-position of pyrimidines under several conditions. However, by applying the lithium–halogen exchange strategy (45) on a protected 5-iodo-$2'$-deoxyurdine, we have successfully incorporated the Te-functionality to the 5-position. We found that the key steps are the transient protection of 5-iodo-$2'$-deoxyuridine derivative **2** as a sodium salt, and the treatment with n-BuLi and $(PhTe)_2$. To the best of our knowledge, we have established the first synthesis of the 5-Te-pyrimidine derivatives.

The synthesis of the 5-TePh-deoxyuridine and 5-TePh-deoxyuridine phosphoramidite is showed in Scheme 1, starting from the silylation of commercially available 5-iodo-$2'$-deoxyuridine derivative **1**. After purification, this intermediate (**2**) was treated with NaH/n-BuLi, followed by adding diphenylditelluride $(PhTe)_2$. This reaction generated an inseparable mixture of the desired 5-PhTe derivative (**6**) and the tentative 6-PhTe derivative (in 10:1 ratio, with 72% yield), along with the reduced byproduct (**8**, in 25% yield). After several failed trials to separate the isomers, such as re-crystallization and very-slow column chromatography, we switched the starting compound to the $3',5'$-di-*O*-silyl derivatives. Unfortunately, this 5-isomer was still difficult to be purified from the 6-regio-isomer. Later, various concentrations of the reactant ($3'$-*O*-silyl-$5'$-DMTr derivative **2**) were tested (Scheme 1). Finally, it was found that when the concentration of the reactant was increased to as high as 0.15 or 0.18 M in THF solution, the 6-TePh isomer could indeed be completely eliminated. Desired 5-Te-isomer **6** was formed as the major product, while **8** was formed as a minor byproduct. Then the desilylation of **6** with TBAF/THF was carried out, generating **7** quantitatively, which was finally converted into 5-phenyltelluro thymdine (^{Te}T) phosphoramidite (**10**) for solid phase synthesis of the Te-DNA. The characteristic distributions of the tellurium isotopes in mass spectra of **6**, **7** and **10** were observed and confirmed the incorporation of the Te-functionality.
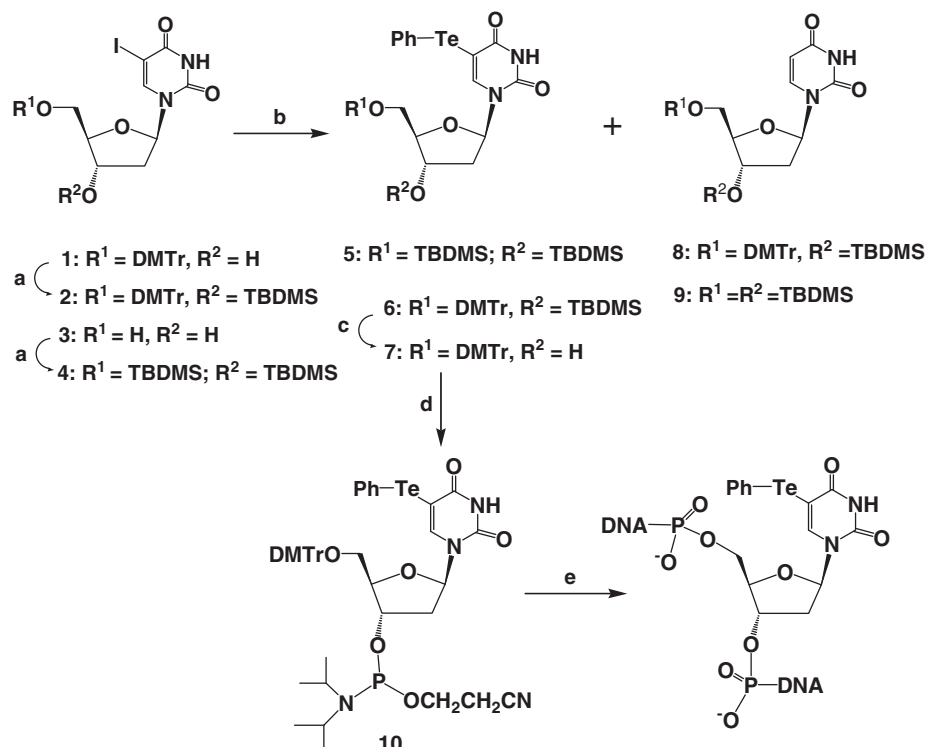
Scheme 1. Synthesis of the 5-phenyltelluro-2′-deoxyuridine, its phosphoramidite, and the Te-DNAs. (**A**) TBDMS-Cl, Im., DMF, 4 h, room temperature (RT); (**B**) (i) NaH, THF, 15 min, RT; (ii) *n*-BuLi, THF, 10 min, −78°C; (iii) Ph$_2$Te$_2$, 1 h, −78°C; (**C**) TBAF, THF, 4 h, RT; (**D**) i-Pr$_2$NP(Cl)CH$_2$CH$_2$CN, DIEA, CH$_2$Cl$_2$, 1 h, RT; (**E**) the solid-phase synthesis.
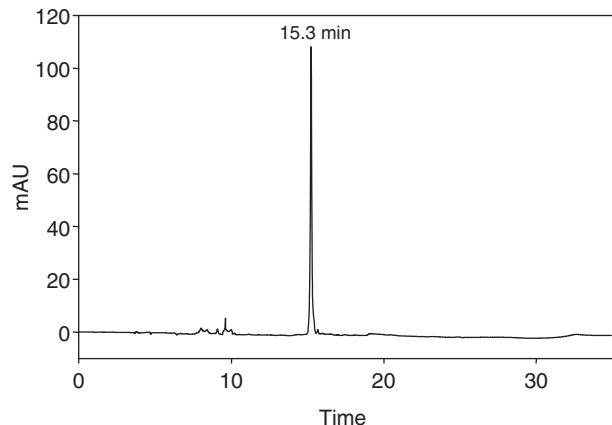
Figure 1. HPLC analysis of 5-TePh-9-mer: [5′-DMTr-ATGG (5-TePh-T)GCTC-3′]. HPLC conditions: Welchrom C18-XB column (4.6 × 250 mm, 5 μ), 25°C, 1 ml/min, gradient from buffer A to 90% buffer B in 20 min. The retention time of the full-length sample is 15.3 min.

Table 1. MALDI-TOF MS of the Te-derivatized DNA oligonucleotides

Entry	DNA sequences	Measured (calcd) *m/z*
1	ATGG(^{Te}T)GCTC	[M]$^-$: 2919.3 (2919.5)
	C$_{93}$H$_{114}$N$_{32}$O$_{54}$P$_8$Te	
2	CTCCCA(^{Te}T)CC	[M]$^-$: 2784.4 (2784.4)
	C$_{89}$H$_{113}$N$_{27}$O$_{53}$P$_8$Te	
3	CT(^{Te}T)CTTGTCCG	[M]$^-$: 3464.5 (3463.8)
	C$_{111}$H$_{140}$N$_{32}$O$_{69}$P$_{10}$Te	
4	GCG(^{Te}T)ATACGC	[M+H$^+$]$^+$: 3218.0 (3218.7)
	C$_{102}$H$_{125}$N$_{38}$O$_{58}$P$_9$Te	
5	GTG(^{Te}T)ACAC	[M]$^-$: 2599.4 (2599.3)
	C$_{83}$H$_{101}$N$_{30}$O$_{46}$P$_7$Te	
6	G(2′-Se-dU)G(^{Te}T)ACAC	[M+H$^+$]$^+$: 2679.2 (2679.2)
	C$_{83}$H$_{101}$N$_{30}$O$_{46}$P$_7$SeTe	

Synthesis of the 5-Te-functionalized DNA

Considering that the Te-functionality is electron rich, its oxidative removal might happen during solid-phase synthesis and purification. Fortunately, this Te-phosphoramidite is well compatible with the solid-phase synthesis conditions, thereby being incorporated into several designed DNA sequences. After K$_2$CO$_3$ (0.05 M in MeOH) cleavage and deprotection, the crude DNA solution was analyzed by analytical RP-HPLC. As showed in Figure 1, the coupling yield is over 95%.
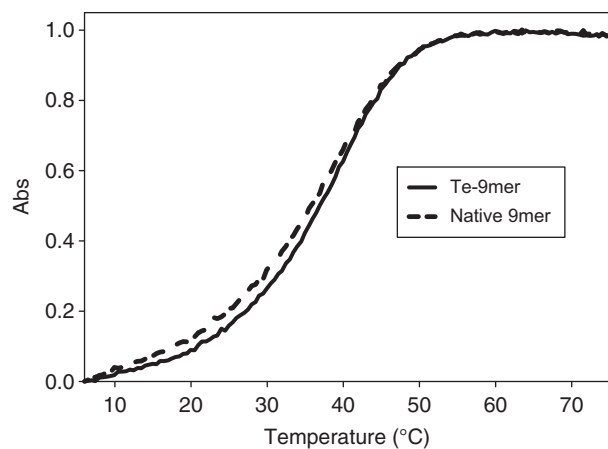
The synthesized Te-DNAs were then purified in a preparative RP-HPLC system in trityl-on form. After treated with 3% trichloroacedic acid for 2 min, the solution was neutralized with triethylamine and extracted with petroleum ether, followed by the second purification in trityl-off form. All the Te-modified DNA oligonucleotides were characterized by MALDI-TOF, and several Te-DNA oligonucleotides were listed in Table 1.

Thermodenaturization study of oligonucleotide duplexes containing the 5-Te derivatization

To evaluate the potential structure perturbation caused by this bulky tellurium moiety (Ph–Te), we conducted the UV–thermal denaturation studies. Our experimental

Table 2. UV-melting study of the Te-DNA duplexes

Entry	DNA duplex	T_m (°C)
1	5′-ATGG(^{Te}T)GCTC-3′ 3′-TACCACGAG-5′	40.3 ± 0.2
2	5′-ATGGTGCTC-3′ 3′-TACCACGAG-5′	39.8 ± 0.3
3	5′-CT(^{Te}T)CTTGTCCG-3′ 3′-GAAGAACAGGC-5′	44.1 ± 0.3
4	5′-CTTCTTGTCCG-3′ 3′-GAAGAACAGGC-5′	44.0 ± 0.2

Table 3. X-ray data collection: the data collected at selenium K-edge

Data collection	$\lambda = 0.9795$ Å
Resolution range, Å (last shell)	18.89–1.50 (1.55–1.50)
Unique reflections	3659
Completeness (%)	94.4
R_{merge} (%)	7.5 (42.7)
$\langle I/\sigma(I)\rangle$	14.9 (2.4)
Redundancy	8.63 (5.30)
Reduced chi-squared	0.93 (0.42)

$R_{merge} = \Sigma|I - \langle I\rangle|/\Sigma I$.

Figure 2. Normalized thermal–denaturation curves of the native and Te-modified DNA duplexes. The Te-DNA duplex: 5′-ATGG(5-TePh-T)GCTC-3′ and 5′-GAGCACCAT-3′. The solid and dashed curves represent the Te-modified and the corresponding native duplexes with 40.3 ± 0.2 and 39.8 ± 0.3°C as their melting temperatures, respectively.
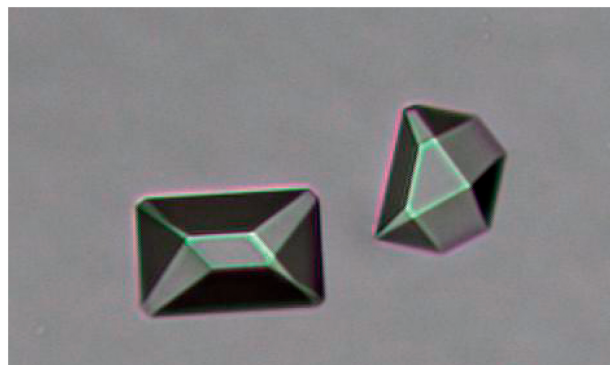
Figure 3. Crystal photo of the Te-DNA octomer [5′-G(2′-SeMe-dU) G(^{Te}T)ACAC-3]$_2$ crystallized in buffer #7 with $0.2 \times 0.1 \times 0.1$ mm in size.

results indicated that the Te-derivatized duplex structures are as stable as the corresponding natives (Table 2 and Figure 2). Clearly, the bulky tellurium substitution does not significantly change the melting temperatures and alter the duplex structure.

Crystallization and data collection of Te-DNA

To further confirm that this 5-TePh modification does not cause obvious structure perturbations, we have carried out the crystallization by using our 2′-Se modification strategy to facilitate the crystal growth (46–48). The modified DNA (5′-G-$^{2'\text{-Se}}$dU-G-^{Te}T-ACAC-3′) was designed, synthesized and purified. Its crystallization conditions were screened with the Hampton Mini-Screening kit. As a result, the Te-DNA crystals were formed in all the 24 buffer conditions of the kit. Moreover, crystals with high-diffraction quality and reasonable sizes were generated in 2 days. Crystals, which formed in buffer #7 of the kit (10% v/v MPD, 40 mM sodium cacodylate pH 6.0, 12 mM spermine tetra–HCl, 80 mM potassium chloride and 20 mM magnesium chloride), were shown in Figure 3 as an example. By the crystal diffraction screening, the crystals formed in buffer #7 were identified to give the highest diffraction resolution (up to 1.50 Å). In addition, several data sets with high diffraction resolution were also collected for further refine purpose. The data collection and refine parameters are listed in Tables 3 and 4.

Crystal structure of the Te-DNA 8-mer

This Te-DNA crystal has the same tetragonal space group P4$_3$2$_1$2 as the corresponding native one (49). The occupancy of Se and Te are 1.0 and 0.35, respectively. The refined B-factor of Se and Te are 28.55 and 23.64, respectively, comparing with other atoms in the structure. The Te-DNA structure (1.50 Å resolution) revealed that both global and local structures of this Te-DNA are virtually identical to the native one (Figure 4A and B), indicating the Te-moiety does not cause significant perturbation. The structure result is also consistent with our biophysical study, suggesting that ^{Te}T and A (Figure 4B and C) pair as well as native T and A. Furthermore, the Te-DNA is stable under a higher temperature. As shown by Figure 5, the Te-DNA was heated at 90°C for 1 h without significant decomposition (<2%). However, since the Te–C bond is sensitive to X-ray irradiation, the occupancy of tellurium (~40%) in the crystal structure is expected. The low electron density of the phenyl group (~16% of expected density) is consistent with cleavage of these two Te–C bonds [Te–C5 and Te–C(Ph)] by the X-ray irradiation. To verify this, the mass analysis of the Te-DNA crystals was carried out. The Te-functionality is stable in the absence of X-ray irradiation, our MS analysis indicated no significant decomposition of the Te-DNA crystals in the crystallization droplet after 3 weeks (Figure 6A). However, after X-ray irradiation, the MALDI-TOF-MS spectra (Figure 6B) showed the loss

of 78 (the phenyl group) and 203.9 mass units (the phenyltelluro group), indicating the partial cleavage of both Te–C bonds by X-ray irradiation.

STM imaging study

Since tellurium atom has the metallic property, we expect that the Te-modified DNA has higher visibility and conductivity under STM imaging than the corresponding

native DNA. To investigate this, we synthesized the Te-DNA [9 nt, 5′-ATGG(^{Te}T)-GCTC-3′, Figure 7], which is complementary to a native DNA [54 nt, 5′-(GA GCACCAT)$_6$-3′] by six repeats, and conducted the STM studies. Interestingly, our experiments revealed that the Te-modified DNA duplex showed much stronger topographic and current peaks (Figure 7A and B) than the corresponding native duplex (Figure 7C and D). Clearly, both the topographic and current images of the Te-duplex showed that the Te-derivatization allowed better
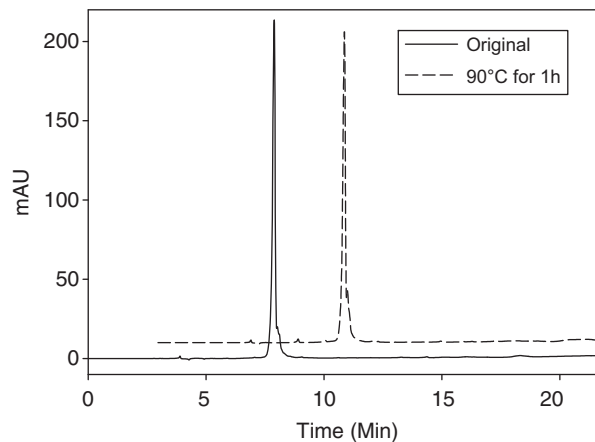
Table 4. Refinement statistics in Te-8-mer

Refinement	
Resolution range, Å (last shell)	25–1.50 (1.55–1.5)
Number of reflections	6859 (424)
R_{work} (%)	19.3
R_{free} (%)	21.5
Number of atoms	
Nucleic Acid (single)	162
Heavy atom	2 (Se, Te)
Water	28
RMSD	
Bond length, Å	0.010
Bond angle	1.73
Average B-factors, Å^2	
All atoms	22.3
Wilson plot	19.6
Overall anisotropic *B*-values	
B11/B22/B33	0.6/0.6/−1.2
Bulk solvent correction	
Solvent density, e/Å^3	0.44
B-factors, Å^2	59.6
Coordinates error (c.-v.), 5 Å	
Esd. from Luzzatt plot, Å	0.17
Esd. from SIGMAA, Å	0.15

Figure 5. The Te-DNA thermal stability and HPLC analysis. Buffer A: 20 mM TEAAc; buffer B: 50% acetonitrile in buffer A. HPLC conditions: Welchrom C18-XB column (4.6 × 250 mm, 5 µ), 25°C, 1 ml/min, gradient from buffer A to 50% buffer B in 15 min. HPLC profiles of Te-DNA [5′-G(2′-SeMe-dU)G(^{Te}T)ACAC-3′] thermal analysis: the solid line (without heating), the dashed line (heated in 10 mM Na-PO$_4$ buffer, pH 7.3, at 90°C for 1 h).

Figure 4. The global and local structures of the Te-DNA duplex [5′-G(2′-SeMe-dU)G(^{Te}T)ACAC-3′]$_2$. The red and yellow balls represent Te and Se atoms, respectively. (**A**) The Te-dsDNA structure (in cyan; 1.50 Å resolution; PDB ID: 3FA1) is superimposed over the native one (in magenta; PDB ID: 1DNS). (**B**) The local structure of the ^{Te}T/A base pair (in cyan) is superimposed over the native T/A base pair (in magenta). (**C**) The experimental electron density (2|F_o| − |F_c| map) of the ^{Te}T/A base pair (σ = 1.0). The green ball represents approximately one-sixth of phenyl group (one carbon).

visualization of the 54-bp DNA duplex (calculated length: 18 nm) with ~20 nm in measured length. Our result also suggested that the native and Te-modified duplexes can assemble with different orientations on the graphite surface, indicated by the topographic and current images of the native and Te-modified duplexes.
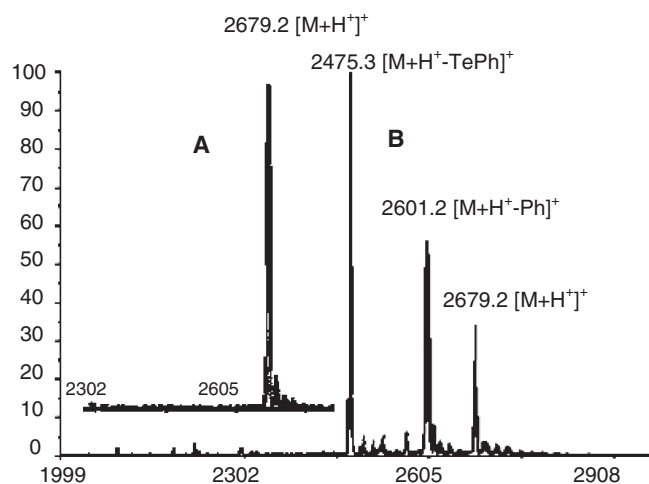

Figure 6. MALDI-TOF mass spectra of the Te-DNA [5′-G (2′-SeMe-dU)G(^TeT)ACAC-3′; molecular formula: $C_{83}H_{101}N_{30}O_{46}P_7$ SeTe; F.W.: 2678.2]. (**A**) The crystal sample without X-ray irradiation; (**B**) the crystal sample with X-ray irradiation.

CONCLUSIONS

In summary, we have first incorporated the Ph–Te-functionality (5-Te) to the 5-position of a pyrimidine, and successfully synthesized the Te-nucleobase-modified nucleoside, phosphoramidite and DNA oligonucleotides. The Te-modified DNA is stable, and the native and modified duplexes have the similar stability. Our biophysical and structural studies indicate that the Te-modified T and A interact as well as native T and A pair, and that the structures of the Te-derivatized and native duplexes are virtually identical. Furthermore, the Te-DNA duplex is readily visible under STM, suggesting a potential strategy to directly image DNA without the structural perturbation. This Te-modification will open a novel research avenue for nucleic acids, including mechanism and function studies, STM imaging and nano-electronic materials.

ACCESSION NUMBER

3FA1.

SUPPLEMENTARY DATA

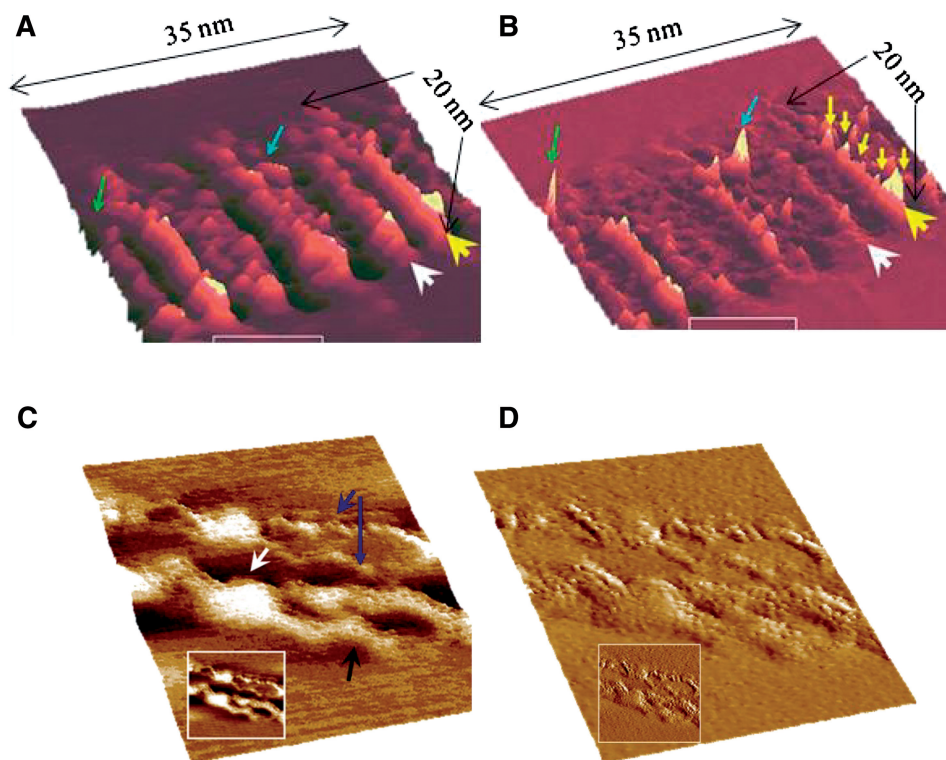Supplementary Data are available at NAR Online.

Figure 7. The STM images of the Te-modified DNA duplex [5′-ATGG(^TeT)-GCTC-3′ and 5′-(GAGCACCAT)_6-3′] and its counterpart native duplex on HOPG. The arrows indicate the edges or current peaks of the measured molecules. (**A**) Topographic image of Te-duplex; (**B**) current image of Te-duplex; (**C**) topographic image of native duplex; (**D**) current image of native duplex. Comparing to the Te-modified DNA duplex, the native sample does not show obvious conductivity. The insets are 2D images corresponding to the 3D images. The sample bias: 0.50 V, the current set point: 100 pA.

REFERENCES

1. Zheng,J., Birktoft,J.J., Chen,Y., Wang,T., Sha,R., Constantinou,P.E., Ginell,S.L., Mao,C. and Seeman,N.C. (2009) From molecular to macroscopic via the rational design of a self-assembled 3D DNA crystal. *Nature*, **461**, 74–77.
2. Xue,X., Wang,F. and Liu,X. (2008) One-step, room temperature, colorimetric detection of mercury (Hg2+) using DNA/nanoparticle conjugates. *J. Am. Chem. Soc.*, **130**, 3244–3245.
3. Rothemund,P.W. (2006) Folding DNA to create nanoscale shapes and patterns. *Nature*, **440**, 297–302.
4. Andersen,E.S., Dong,M., Nielsen,M.M., Jahn,K., Subramani,R., Mamdouh,W., Golas,M.M., Sander,B., Stark,H. and Oliveira,C.L. (2009) Self-assembly of a nanoscale DNA box with a controllable lid. *Nature*, **459**, 73–76.
5. Singer,A., Wanunu,M., Morrison,W., Kuhn,H., Frank-Kamenetskii,M. and Meller,A. (2010) Nanopore based sequence specific detection of duplex DNA for genomic profiling. *Nano Lett.*, **10**, 738–742.
6. Tiemann,K. and Rossi,J.J. (2009) RNAi-based therapeutics-current status, challenges and prospects. *EMBO Mol. Med.*, **1**, 142–151.
7. Huang,Y.C. and Sen,D. (2010) A contractile electronic switch made of DNA. *J. Am. Chem. Soc.*, **132**, 2663–2671.
8. Kratochvilova,I., Kral,K., Buncek,M., Viskova,A., Nespurek,S., Kochalska,A., Todorciuc,T., Weiter,M. and Schneider,B. (2008) Conductivity of natural and modified DNA measured by scanning tunneling microscopy. The effect of sequence, charge and stacking. *Biophys. Chem.*, **138**, 3–10.
9. Ito,T. and Rokita,S.E. (2004) Criteria for efficient transport of excess electrons in DNA. *Angew. Chem. Int. Ed. Engl.*, **43**, 1839–1842.
10. Barnett,R.N., Cleveland,C.L., Joy,A., Landman,U. and Schuster,G.B. (2001) Charge migration in DNA: ion-gated transport. *Science*, **294**, 567–571.
11. Porath,D., Bezryadin,A., de Vries,S. and Dekker,C. (2000) Direct measurement of electrical transport through DNA molecules. *Nature*, **403**, 635–638.
12. Fink,H.W. and Schonenberger,C. (1999) Electrical conduction through DNA molecules. *Nature*, **398**, 407–410.
13. Yang,Z., Chen,F., Chamberlin,S.G. and Benner,S.A. (2010) Expanded genetic alphabets in the polymerase chain reaction. *Angew. Chem. Int. Ed. Engl.*, **49**, 177–180.
14. Hassan,A.E., Sheng,J., Zhang,W. and Huang,Z. (2010) High fidelity of base pairing by 2-selenothymidine in DNA. *J. Am. Chem. Soc.*, **132**, 2120–2121.
15. Egli,M. and Pallan,P.S. (2010) Crystallographic studies of chemically modified nucleic acids: a backward glance. *Chem. Biodivers.*, **7**, 60–89.
16. Ljungman,M. (2009) Targeting the DNA damage response in cancer. *Chem. Rev.*, **109**, 2929–2950.
17. Delaney,J.C., Gao,J., Liu,H., Shrivastav,N., Essigmann,J.M. and Kool,E.T. (2009) Efficient replication bypass of size-expanded DNA base pairs in bacterial cells. *Angew. Chem. Int. Ed. Engl.*, **48**, 4524–4527.
18. Sismour,A.M. and Benner,S.A. (2005) The use of thymidine analogs to improve the replication of an extra DNA base pair: a synthetic biological system. *Nucleic Acids Res.*, **33**, 5640–5646.
19. Kim,T.W., Delaney,J.C., Essigmann,J.M. and Kool,E.T. (2005) Probing the active site tightness of DNA polymerase in subangstrom increments. *Proc. Natl Acad. Sci. USA*, **102**, 15803–15808.
20. Coffer,J.L., Bigham,S.R., Li,X., Pinizzotto,R.F., Rho,Y.G., Pirtle,R.M. and Pirtle,I.L. (1996) Dictation of the shape of mesoscale semiconductor nanoparticle assemblies by plasmid DNA. *Appl. Phys. Lett.*, **69**, 3851–3853.
21. Braun,E., Eichen,Y., Sivan,U. and Ben-Yoseph,G. (1998) DNA-templated assembly and electrode attachment of a conducting silver wire. *Nature*, **391**, 775–778.
22. Ma,Y., Zhang,J., Zhang,G. and He,H. (2004) Polyaniline nanowires on Si surfaces fabricated with DNA templates. *J. Am. Chem. Soc.*, **126**, 7097–7101.
23. Elias,B., Shao,F. and Barton,J.K. (2008) Charge migration along the DNA duplex: hole versus electron transport. *J. Am. Chem. Soc.*, **130**, 1152–1153.
24. Guo,X., Gorodetsky,A.A., Hone,J., Barton,J.K. and Nuckolls,C. (2008) Conductivity of a single DNA duplex bridging a carbon nanotube gap. *Nat. Nanotechnol.*, **3**, 163–167.
25. Sheng,J., Hassan,A.E. and Huang,Z. (2008) New telluride-mediated elimination for novel synthesis of 2′,3′-didehydro-2′,3′-dideoxynucleosides. *J. Org. Chem.*, **73**, 3725–3729.
26. Sheng,J., Hassan,A.E. and Huang,Z. (2009) Synthesis of the first tellurium-derivatized oligonucleotides for structural and functional studies. *Chem. Eur. J.*, **15**, 10210–10216.
27. Moroder,L. (2005) Isosteric replacement of sulfur with other chalcogens in peptides and proteins. *J. Pept. Sci.*, **11**, 187–214.
28. Sheng,J. and Huang,Z. (2008) Selenium derivatization of nucleic acids for phase and structure determination in nucleic acid X-ray crystallography. *Int. J. Mol. Sci.*, **9**, 258–271.
29. Otwinowski,Z. and Minor,W. (1997) Processing of X-ray diffraction data collected in oscillation mode. *Method. Enzym.*, **276**, 307–326.
30. McCoy,A.J., Grosse-Kunstleve,R.W., Adams,P.D., Winn,M.D., Storoni,L.C. and Read,R.J. (2007) Phaser crystallographic software. *J. Appl. Crystallogr.*, **40**, 658–674.
31. Brunger,A.T., Adams,P.D., Clore,G.M., DeLano,W.L., Gros,P., Grosse-Kunstleve,R.W., Jiang,J.S., Kuszewski,J., Nilges,M., Pannu,N.S. *et al.* (1998) Crystallography & NMR system: A new software suite for macromolecular structure determination. *Acta Crystallogr. D Biol. Crystallogr.*, **54**, 905–921.
32. Murshudov,G.N., Vagin,A.A. and Dodson,E.J. (1997) Refinement of macromolecular structures by the maximum-likelihood method. *Acta Crystallogr. D Biol. Crystallogr.*, **53**, 240–255.
33. Parkinson,G., Vojtechovsky,J., Clowney,L., Brunger,A.T. and Berman,H.M. (1996) New parameters for the refinement of nucleic acid-containing structures. *Acta Crystallogr. D Biol. Crystallogr.*, **52**, 57–64.
34. Brunger,A.T. (1992) Free R value: a novel statistical quantity for assessing the accuracy of crystal structures. *Nature*, **355**, 472–475.
35. Read,R.J. (1986) Improved Fourier coefficients for maps using phases from partial structures with errors. *Acta Cryst. A*, **42**, 140–149.
36. Rose,F., Martin,P., Fujita,H. and Kawakatsu,H. (2006) Adsorption and combing of DNA on HOPG surfaces of bulk crystals and nanosheets: application to the bridging of DNA between HOPG/Si heterostructures. *Nanotechnology*, **17**, 3325–3332.
37. Naganara,L.A., Thundat,T. and Lindsay,S.M. (1989) Preparation and characterization of STM tips for electrochemical studies. *Rev. Sci. Instrum.*, **60**, 3128–3130.

38. Schinazi,R.F., Arbiser,J., Lee,J.J., Kalman,T.I. and Prusoff,W.H. (1986) Synthesis and biological activity of 5-phenylselenenyl-substituted pyrimidine nucleosides. *J. Med. Chem.*, **29**, 1293–1295.

39. Bergstrom,D., Beal,P., Husain,A., Lind,R. and Jenson,J. (1989) Palladium-mediated coupling between organic disulfides and nucleic acid constituents. *J. Am. Chem. Soc.*, **111**, 374–375.

40. Hirota,K., Tomishi,T., Maki,Y. and Sajiki,H. (1998) Synthesis of 5-arylthiouridines via electrophilic substitution of 5-bromouridines with diaryl disulfides. *Nucleosides, Nucleotides and Nucleic Acids*, **17**, 161–173.

41. Zeng,Y., Cao,H. and Wang,Y. (2006) Facile Photocyclization Chemistry of 5-Phenylthio-2'-deoxyuridine in Duplex DNA. *Organic Lett.*, **8**, 2527–2530.

42. Lee,C. and Kim,Y. (1991) Direct regioselective arylsulfenylation and arylselenenylation at 5-position of uracils mediated by silver reagents. *Tetrahedron Lett.*, **32**, 2401–2404.

43. Ahmadian,M., Zhang,P. and Bergstrom,D.E. (1998) A comparative study of the thermal stability of oligodeoxyribonucleotides containing 5-substituted 2'-deoxyuridines. *Nucleic Acids Res.*, **26**, 3127–3135.

44. Hayakawa,H., Tanaka,H., Obi,K., Itoh,M. and Miyasaka,T. (1987) A simple and general entry to 5-substituted uridines based on regioselective lithiation controlled by a protecting group in the sugar moiety. *Tetrahedron Lett.*, **28**, 87–90.

45. Karino,N., Ueno,Y. and Matsuda,A. (2001) Synthesis and properties of oligonucleotides containing 5-formyl-2'-deoxycytidine: in vitro DNA polymerase reactions on DNA templates containing 5-formyl-2'-deoxycytidine. *Nucleic Acids Res.*, **29**, 2456–2463.

46. Jiang,J., Sheng,J., Carrasco,N. and Huang,Z. (2007) Selenium derivatization of nucleic acids for crystallography. *Nucleic Acids Res.*, **35**, 477–485.

47. Salon,J., Sheng,J., Gan,J. and Huang,Z. (2010) Synthesis and crystal structure of 2'-se-modified guanosine containing DNA. *J. Org. Chem.*, **75**, 637–641.

48. Sheng,J., Salon,J., Gan,J. and Huang,Z. (2010) Synthesis and crystal structure study of 2'-Se-adenosine-derivatized DNA. *Sci. China: Chem.*, **53**, 78–85.

49. Jain,S., Zon,G. and Sundaralingam,M. (1989) Base only binding of spermine in the deep groove of the A-DNA octamer d(GTGT ACAC). *Biochemistry*, **28**, 2360–2364.